

# Bio-Macromolecular Surface Coatings for Autohesive, Transparent, Elastomeric Foils

Maria G. Bauer and Oliver Lieleg\*

Thin materials made from elastomeric polymers such as polydimethylsiloxane (PDMS) and polyurethane (PU) can be both, compliant and resilient. Their mechanical robustness and flexibility will make them great candidates for applications in the human body where space is limited and repeated deformations occur. Nonetheless, current medical applications of elastomeric foil-like products are mainly restricted to inflatable balloon parts of stents or intubation tubes. Here, a key limiting factor is the autohesive behavior of those foils, that is, their propensity to stick to themselves. This property impedes handling and processing and can also interfere with the designated tasks of such foils. To mitigate this undesired behavior, different bio-macromolecular coatings are applied here and assess their influence on the autohesive behavior, flexibility, and transparency of the materials. A non-covalent, dopamine-assisted coating approach is compared to a covalent coating strategy employing carbodiimide chemistry and investigated both, anionic and cationic macromolecules as top layers. The results show that especially the carbodiimide-mediated mucin coating can efficiently suppress the autohesive behavior of the foils while maintaining the flexibility and transparency of the material. Thus, such coatings can not only broaden the medical application range of foil-based elastomeric devices but may also prove beneficial for applications in soft robotics.

optical appearance of the product,<sup>[1]</sup> coatings are mainly applied to protect the bulk material from undesired environmental impacts, for example, from corrosion,<sup>[2]</sup> wear,<sup>[3,4]</sup> heat damage,<sup>[5]</sup> cellular or bacterial colonization,<sup>[6a,6b,7]</sup> or to activate the surface so it gains additional functionalities. Examples of such surface-associated functionalities are catalysis<sup>[8]</sup> and filtering tasks,<sup>[9]</sup> local drug release,<sup>[10]</sup> control over cellular adhesion,<sup>[7,11]</sup> as well as photo- and thermochromic<sup>[12]</sup> or self-healing properties.<sup>[13]</sup> Thus, coatings are employed in almost any kind of industry, ranging from aeronautic and automotive applications,<sup>[14]</sup> over materials used in construction and infrastructure,<sup>[15]</sup> to a broad range of problems in biochemical, medical, and pharmaceutical areas.<sup>[16a–d,17]</sup> In addition, coatings can play an important role in achieving more environmentally friendly and sustainable products. Examples include energy-efficient paintings/coatings for buildings,<sup>[18]</sup> coatings improving the efficiency of photovoltaic systems and batteries,<sup>[19]</sup> coatings to enhance the function of filters and membranes for water

and air cleaning purposes,<sup>[20]</sup> coatings prolonging the lifetime of a product.<sup>[21]</sup>

For medical purposes, but also when targeting pharmaceutical applications or developing biocompatible surfaces on synthetic materials, biomacromolecules are frequently chosen as top-layer molecules in coatings. In addition to being well biocompatible, those large and often very complex molecules can come with a variety of beneficial properties, such as antimicrobial activity, lubricious behavior, the ability to hold and release bioactive molecules, and to enhance/weaken cell adhesion.<sup>[17]</sup> Especially when dealing with medical devices, a biomacromolecule coating created on the product surface can establish such beneficial multifunctionality on the device.


The range of materials used in the medical field is broad as it includes ceramics, metals, and polymeric materials. For many reasons, however, polymeric materials are often preferred. For instance, thin polymeric products such as foils can be both, transparent and flexible, and this enables a range of applications for which metals and ceramics are inappropriate. Two examples of such elastomeric polymer materials frequently used in the biomedical field are polydimethylsiloxane (PDMS) and polyurethane (PU). Since these materials combine different ben-

## 1. Introduction

Applying coatings to surfaces is a ubiquitous tool to adjust the surface properties of a material. In addition to changing the

M. G. Bauer, O. Lieleg  
School of Engineering and Design  
Department of Materials Engineering  
Technical University of Munich  
Boltzmannstraße 15, 85748 Garching, Germany  
E-mail: oliver.lieleg@tum.de

M. G. Bauer, O. Lieleg  
Center for Protein Assemblies and Munich Institute of Biomedical Engineering  
Technical University of Munich  
Ernst-Otto-Fischer Str. 8, 85748 Garching, Germany

 The ORCID identification number(s) for the author(s) of this article can be found under <https://doi.org/10.1002/mame.202200681>

© 2023 The Authors. Macromolecular Materials and Engineering published by Wiley-VCH GmbH. This is an open access article under the terms of the Creative Commons Attribution License, which permits use, distribution and reproduction in any medium, provided the original work is properly cited.

DOI: 10.1002/mame.202200681

eficial properties, they are used in a broad range of applications. Whereas PDMS is used, for example, for catheters, micropumps, bandages, and implants.<sup>[22]</sup> PU has previously been applied as a coating to create antibacterial surfaces, to fabricate drug delivery vehicle, stents, surgical dressings, tissue engineering scaffolds, and cardiac patches.<sup>[23]</sup> However, thin polymeric foils typically also come with an issue: they tend to be quite adhesive to other materials and to themselves, the latter of which is a mechanism typically referred to as autohesion.<sup>[24]</sup> Handling or processing such autohesive foils is challenging, and this particular material property sometimes also interferes with the intended function of the foils: intravenous bags and the inflatable balloon parts of stents or intubation tubes would open up more easily if the polymer material would be less sticky. Similarly, fluidic elastomeric actuators (FEA), a very adaptive type of actuator used for soft robotics, could benefit from such coatings as well. Those FEAs comprise thin structural compartments made of elastomeric polymers which are actuated by changing the internal pressure—either by pneumatic or hydraulic means. Here, every time the chambers are deflated, the elastomeric walls of the chambers repeatedly come into contact with each other, and autohesive properties are undesired here. Of course, the application range of such FEAs is not limited to medical devices such as endoscopes; they are anticipated to be particularly suitable for applications promoting active safety in automotive, in industrial applications, and for haptic-interface tasks.<sup>[25]</sup> Overall, the current application range of polymer foils would certainly be extended if the autohesion of the foils could be mitigated—without losing the flexibility and transparency of the thin polymer material. Here, applying macromolecular coatings might be a good solution to achieve this goal.

Compared to the bulk material of a product, coatings are typically very thin. They rarely exceed a thickness of a few hundred micrometers, and they can even be constituted by a single monolayer of (macro)molecules.<sup>[26]</sup> Nonetheless, whenever coatings are applied, the idea is that the surface properties of the material are afterwards dominated by the coating—and that the coating does not influence the bulk properties of the material. If the coating procedure requires multiple treatment steps, it is expected that the last, final treatment creating the top layer of the coating is most important—and any influence the potential intermediate layers might have, is typically not investigated in detail.

In the past, two coating strategies were mainly put forward to immobilize biomacromolecules onto products. The first coating strategy, a carbodiimide-mediated coating process, is well established, frequently used, and creates covalent bonds between the substrate, the intermediate layer, and the top-layer of the coating. This strategy, however, can only be applied to certain materials, which limits its use. In contrast, the second coating strategy, a dopamine-assisted process, is comparably new and establishes an adhesive, intermediate layer on a very broad range of materials; with this approach, attaching a macromolecular top layer based on a combination of covalent and non-covalent bonds is very easily possible.<sup>[27]</sup>

Here, we ask how macromolecular coatings generated with either of the two coating strategies mentioned above affect the material properties of transparent, flexible polymer foils made from carbonate-based polyurethane (PCU) and PDMS, respectively. As biomacromolecules forming the top layer of the coat-

ings, we select examples that come with different charge states: first, manually purified mucins, which are poly-anionic glycoproteins with a molecular weight (MW) of a few megadaltons; second, two dextrans variants, that is, synthetic polysaccharides, with a molecular weight of MW = 150 kDa that are functionalized with cationic residues (either with quaternary amine groups or with the cationic amino acid lysine). Then, we compare a range of material properties for coated and uncoated foils, including their flexibility, transparency, and autohesive behavior, and relate them to alterations in wettability, surface potential, and (putatively) surface roughness as brought about by the coating application.

## 2. Results and Discussion

For all following results two different materials, that is, polydimethylsiloxane (PDMS) and carbonate-based polyurethane (PCU), are tested either uncoated or coated with mucins, Lysine-Dextrans (LDex), or Q-Dextrans (QDex) via either a carbodiimide-mediated strategy (carbo) or a dopamine-based strategy (dopa). To clearly identify the different material/coating combinations studied in this manuscript, they will be referred to as follows: “material”—“coating strategy”—“top-layer molecule” with PCU/PDMS, uncoated/carbo/dopa, and mucin/LDex/QDex as alternatives for the respective sections.

As depicted in **Figure 1**, both foil materials tested here exhibit (in their untreated form) hydrophobic properties as indicated by contact angle (CA) values above 90°: we measure 113° ± 2° for PDMS and 107° ± 2° for PCU. However, the surface wettability of both materials should be considerably altered by applying a macromolecular coating. In fact, three different aspects of the two coating strategies tested here can contribute to rendering the base materials more hydrophilic: the plasma activation (which is the first step of the carbodiimide-based coating process), the dopamine pre-coating, as well as the mostly hydrophilic structures of the selected macromolecules.<sup>[28]</sup> And indeed, all tested surface coatings can reduce the CA of the foils—at least to some extent (**Figure 1**). On PDMS (**Figure 1a**), the hydrophilizing effect achieved with the two mucin coatings is clearly stronger than the effect obtained with the two dextran coatings. Probably, owing to their much larger molecular weight, the mucins (MW ≈ 4–6 MDa) can alter the surface properties of the material more efficiently than the smaller dextrans (MW = 150 kDa). Such a clear difference between the different coatings is, however, not visible for PCU (**Figure 1b**). Maybe here, on a material that is less hydrophobic than PDMS, the smaller dextrans are sufficient to achieve a similarly strong hydrophilization as the larger mucins.

Of course, whereas a change in the wetting behavior of the foils is a clear indication that the surface treatment has worked, this result may not correlate with a putative alteration in the autohesive properties of a foil (which typically occur in the dry state of a foil). Thus, we next compare the strength of these autohesive properties of differently coated foils to that of their uncoated counterparts. To do so, two different pulling tests are conducted, in which the orientation of the pulling direction with respect to the contact interface of two foil samples differs: As depicted in the schematics of **Figure 2a,b**, lap shear tests probe a configuration where the pulling force is applied in parallel to the sample interface (**Figure 2a**); in contrast, in detachment tests, the pulling force is orientated orthogonally to the interface (**Figure 2b**).

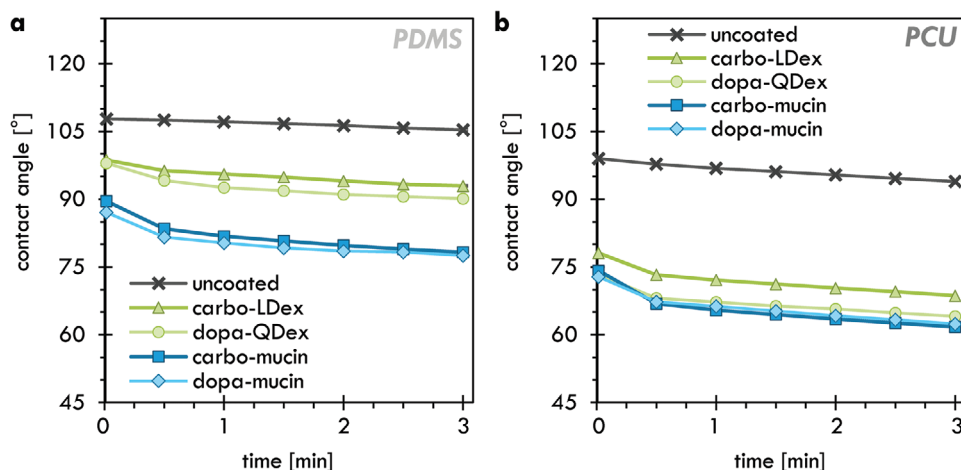


**Figure 1.** Influence of surface modifications on the wettability of PDMS and of PCU foils. The development of the water CA determined on uncoated (cross symbols), carbo-LDex coated (triangles), dopa-QDex coated (circles), carbo-mucin coated (squares), and dopa-mucin coated (diamonds) surfaces of a) PDMS samples and b) PCU samples is shown over a time period of 3 min. The error bars depict the error of the mean determined from at least 10 samples. If no error bars are visible, they are in the range of the size of the symbols.

The results in Figure 2c show that all coating variants—partial and full coatings—slightly increase the resistance of the PDMS foils against lap shear movement (compared to uncoated PDMS foils); however, no difference was found between the base coated samples (i.e., carbo coated and dopa coated) and their corresponding fully coated counterparts. For the “dopa”-based coatings, one explanation for this outcome could be that, at some spots of the interface, the sticky dopamine layer is not entirely covered by the top layer of macromolecules. However, for the “carbo”-based coatings, such an explanation does not apply. Interestingly, the results we obtain for the detachment tests (Figure 2d) indicate the opposite behavior, that is, a significant reduction in the detachment resistance—at least for the full “carbo”-coatings. Additionally, here, a significant difference between the results of each intermediate step and the corresponding completed coatings was observed, indicating that PDMS-carbo and PDMS-dopa foils exhibit a stronger autohesive behavior than fully coated PDMS foils.

For PCU samples (Figure 2e, f), the observed behavior follows the same trend as for the detachment tests conducted with PDMS samples. Here, both in the lap shear tests (Figure 2e) as well as in the detachment tests (Figure 2f), the “carbo”-coatings significantly decrease the resistance of the material towards the respective movement. For the carbo-mucin coating, this effect is even so strong that the two foil samples sometimes spontaneously separate before the lap shear measurement can be started. Because of this behavior, the number of measuring points we report for the PCU-carbo-mucin samples is lower than for the other samples, and the determined value should be interpreted as an upper limit rather than a real average. A similar effect is observed for the PCU-carbo-LDex samples as well as PCU-carbo samples; however, here, it occurred less frequently. Owing to this complication, which affects the comparability of the sample sets, the horizontal lines indicating significant differences in Figure 2e are dashed. In contrast, we did not find a significant difference between the results obtained for samples fully treated with the dopamine-based coating strategy compared to those obtained for

the uncoated materials, but such a difference was observed between the dopa-coated and the dopa-QDex coated as well as the dopa-LDex coated samples. In the detachment tests (Figure 2f), such a premature separation of the samples is technically not possible, but the overall trend is similar to the behavior observed in the lap shear tests: the “carbo”-coatings significantly reduce the resistance to lap shear and detachment, respectively, whereas the “dopa”-coatings do not. Moreover, we note that the values obtained for the PCU-carbo-mucin samples are extremely low, that is, two to three orders of magnitude smaller than those determined for uncoated samples. We speculate that a combination of two effects might be responsible for the observed behavior. First, the more efficient hydrophilization obtained for the mucin coatings (see Figure 1) indicates a more efficient surface coverage achieved with this particular macromolecule; second, the larger mucins might generate a stronger steric hindrance effect compared to the smaller dextrans. The latter might reduce the probability that a local, uncovered spot of the sticky dopamine layer can get in direct contact with the opposing sample surface thus decreasing its detachment resistance.

To further investigate those somewhat unexpected results, we determine the zeta potentials of the surfaces of the differently coated and uncoated foils. All uncoated materials are clearly negatively charged; we measure  $-45 \text{ mV} \pm 0.6 \text{ mV}$  for PDMS (Figure 3a, left) and  $-41 \text{ mV} \pm 2 \text{ mV}$  for PCU (Figure 3a, right). Based on the structural formulas of the polymers comprising those foils, finding such strongly anionic properties is not obvious (especially for the PDMS samples, which contain mostly uncharged and non-polar methyl groups). However, a similar behavior has been observed previously on PDMS<sup>[29]</sup> as well as on other solid surfaces which were anticipated to be inert due to the lack of ionizable surface groups.<sup>[30,31]</sup> There, this behavior was rationalized by an asymmetric adsorption of water ions; however, the origin of this effect and whether hydroxide ions or hydronium ions show a higher affinity towards the polymeric surface is still under discussion.<sup>[31,32]</sup> In the presence of the full coating, those surface zeta potentials should be changed—and both, the respec-

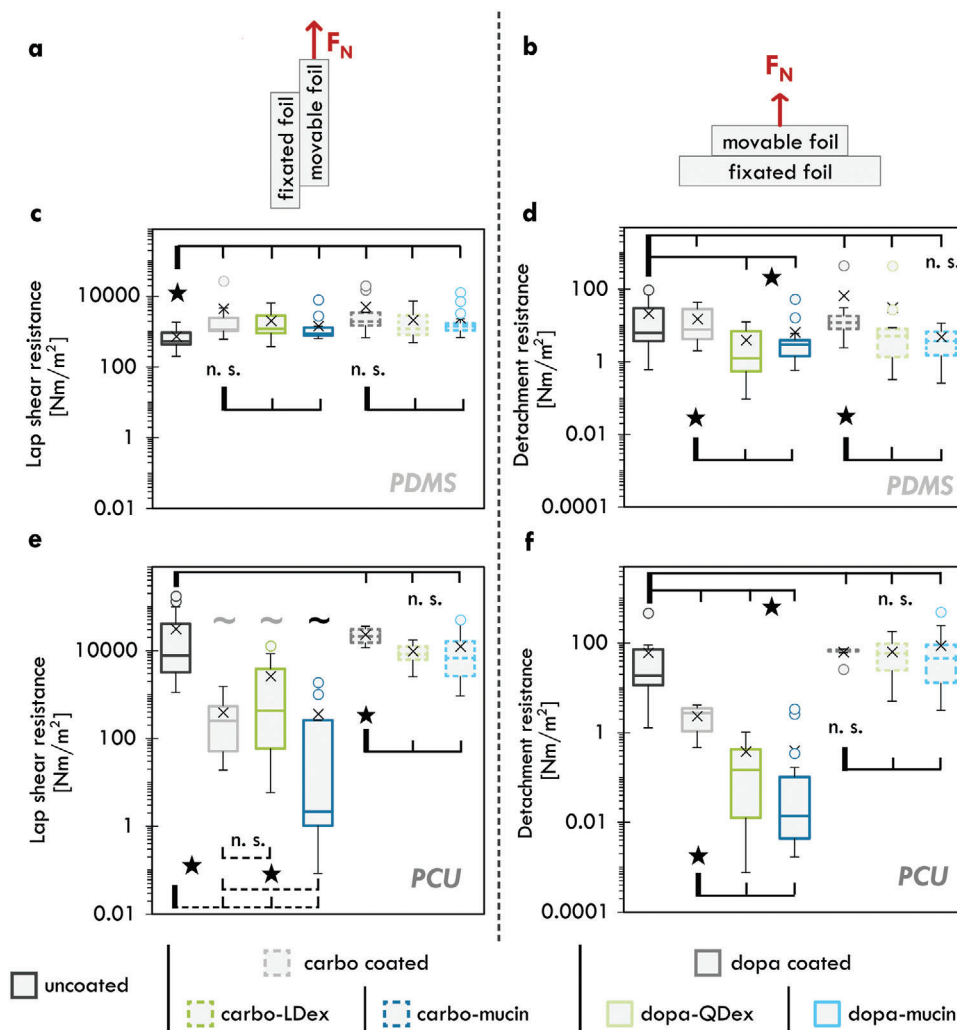


**Figure 2.** Resistance of (surface modified) foils against lap shear and detachment. a,b) Schematics depicting the two pulling modes tested here. For the lap shear tests (a, c, e), a force was applied parallel to the interface of the two foils; for the detachment tests (b, d, f), a force was applied orthogonally to the interface. c,e) Results of the lap shear tests. The tilde symbols in d) mark conditions where some sets of foils detached before the measurements could be started (grey tilde: 20% of the test sets; black tilde: 50% of the test sets). d,f) Results of the detachment tests. All diagrams display data obtained for uncoated samples (black lines), carbo coated samples (full grey lines), carbo-LDex coated samples (full green lines), carbo-mucin coated samples (full blue lines), dopa coated samples (dashed grey lines), dopa-QDex coated samples (dashed green lines), and dopa-mucin coated samples (dashed blue lines). The boxes denote the median (central line), the median plus the first quartile (top line), and the median minus the third quartile (bottom line) as determined for at least 8 sample sets. Cross symbols indicate the mean, and circles depict outliers based on an outlier multiplier of 2.2. Asterisks indicate significant differences ( $p = 0.05$ ) and n.s. indicates that no significant difference was found. The legend at the bottom of the figure applies to all diagrams.

tive pre-treatment (dopamine incubation vs plasma activation/vs silane coupling) as well as the macromolecule used for creating the top layer in the coating should have an influence here. Ideally, the surface properties of the foil would become clearly dominated by the properties of the macromolecule used; and zeta potential measurements conducted on macromolecular solutions containing either mucin, QDex, or LDex (which are all conducted at identical conditions to ensure comparability, that is, at a pH value of  $\approx 5.6$  and in the presence of 1 mM KCl) clearly show that those macromolecules have very different charge states (Figure 3b): mucin ( $-28 \text{ mV} \pm 0.3 \text{ mV}$ ) is clearly anionic, QDex ( $13 \text{ mV} \pm 4 \text{ mV}$ ) is clearly cationic, and LDex ( $-1 \text{ mV} \pm 0.3 \text{ mV}$ ) is almost uncharged at this pH value.

Dopamine carries an amine group and thus is cationic; therefore, applying a dopamine pre-coating should render the foils less anionic. On PDMS, this alteration in the surface charge state induced by dopamine is only small (Figure 3c); in contrast, we find a strong shift by 25 mV for the PCU foils (Figure 3d). For the full, dopamine-assisted coatings generated on PDMS, we find very similar values as for the dopamine pre-coating alone.

Apparently, the surface properties of PDMS are—in terms of charge—so strong that it is not easily possible to override them with a macromolecular coating as we attempt it here. On the PCU samples, however, either macromolecule entails a strong change in the surface charge state, and the obtained result agrees with those of the macromolecules used: Attaching the QDex

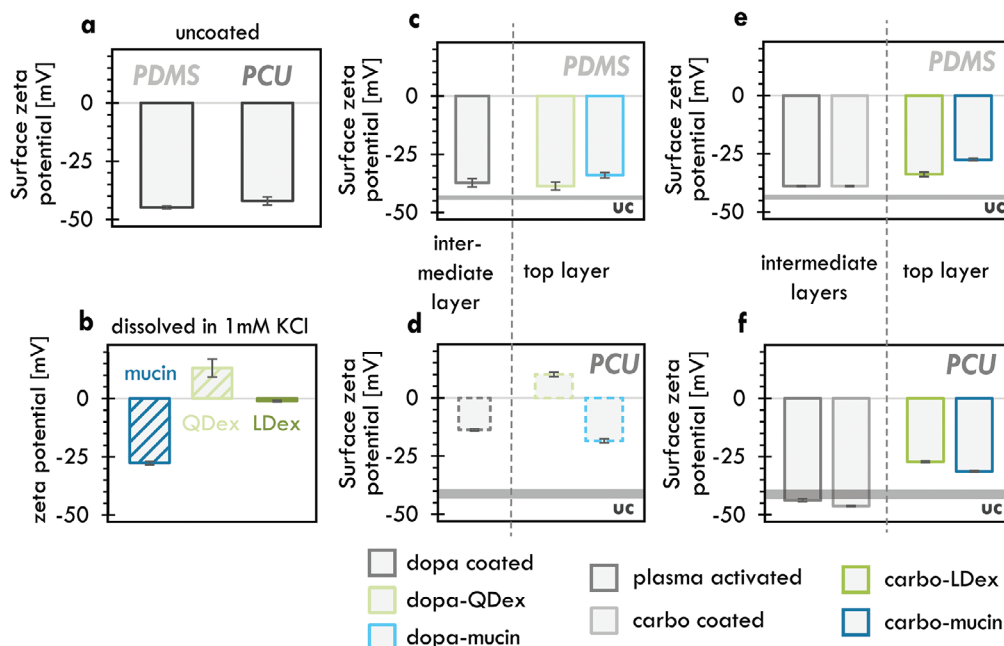


**Figure 3.** Zeta potentials of bare and coated substrate materials as well as of the molecules used as top layers in the coatings. All values shown were determined at a pH value of 5.6. a) Surface potentials of the uncoated (uc) materials. b) Zeta potentials of the macromolecules used as top-layers. c,d) Results obtained for the dopamine-based coating strategy. e,f) Results obtained for the carbodiimide-mediated coating strategy. The grey bar labeled with “uc” in diagrams (c–f) indicates results obtained for the uncoated substrate as displayed in (a). The legend at the bottom of the figure applies to diagrams (c–f). Error bars depict the error of the mean as determined from at least 3 (sets of) samples. If no error bars are visible, they are in the range of the size of the symbols.

molecules leads to an overall cationic surface whereas attaching the mucins leads to an anionic surface, which is (in absolute numbers) less strongly charged than pure PCU itself. However, neither of the two coatings fully reach the zeta potential values we determined for the corresponding macromolecule in solution. This indicates that, even if a rather efficient coating is created, the intermediate dopamine layer still affects the surface properties of the coating.

For the carbodiimide-mediated coating process, the two preconditioning steps seem to have only minor influences on the measured zeta potential, and this holds true for both foil materials tested here (Figure 3e,f). However, when the full coatings are applied, we do find relevant alterations in the measured surface zeta potentials. When using mucins as a top layer molecule, the measured surface potentials are very similar to that of mucins in solution, indicating a very efficient alteration of either foil surface by the carbodiimide-mediated coating strategy. When using LDex molecules for those covalent coatings, the obtained surface potentials are still strongly anionic and comparable to those achieved with mucins. However, the measured values are “less negative” than those obtained for “incomplete” coatings carrying the pre-conditioning, intermediate layers only. In other words, also here, attaching the final macromolecule layer has a clear influence on the final surface potential of the material.

So far, mainly desired alterations of surface properties as induced by the different coatings were examined; however, surface coatings might also lead to undesired changes of certain surface properties (e.g., the surface roughness) or they could even negatively impact the bulk behavior of the sample—and neither is

typically desired. Accordingly, when modifying the surfaces of a foil, it is crucial that the other characteristic properties of the material, that is, its transparency and flexibility, are maintained. Ideally, of course, the applied coatings were to only alter the surface properties of the foils, but this needs to be verified. Therefore, in another set of tests, we ask if the desirable material properties of PDMS and PCU foils are affected by the different coatings investigated here.

First, the transparency of foils with and without coatings is compared by quantifying their absorbance behavior in the UV-vis range, that is, between wavelengths of 190 to 900 nm (Figure 4a,b). Importantly, we find that none of the coatings alters the transparency of PDMS or PCU foils in a considerable manner.

This good transparency of both, PDMS and PCU foils, agrees with the very low surface roughness values (the root-mean-square-height  $S_q$  and the developed interfacial ratio  $S_{dr}$ ) we determine for them using laser scanning profilometry: we obtain  $S_{q,PDMS} = (0.4 \pm 0.2) \mu\text{m}$  and  $S_{q,PCU} = (0.2 \pm 0.1) \mu\text{m}$ , as well as  $S_{dr,PDMS} = (1 \pm 1) \%$  and  $S_{dr,PCU} = (0.6 \pm 0.2) \%$  (Figure 4c,d,f,g). After applying the different coatings, these roughness values remain in a very similar range. Additionally, we find very similar  $S_{pc}$  values for coated and uncoated samples (and this holds true for both foil materials investigated here). As this particular metrological parameter quantifies the curvature of peak structures on the surface, this finding suggests that the different coating procedures do not entail a local accumulation of chemicals/molecules (especially dopamine is known for forming agglomerates) but rather lead to spatially homogenous coatings.

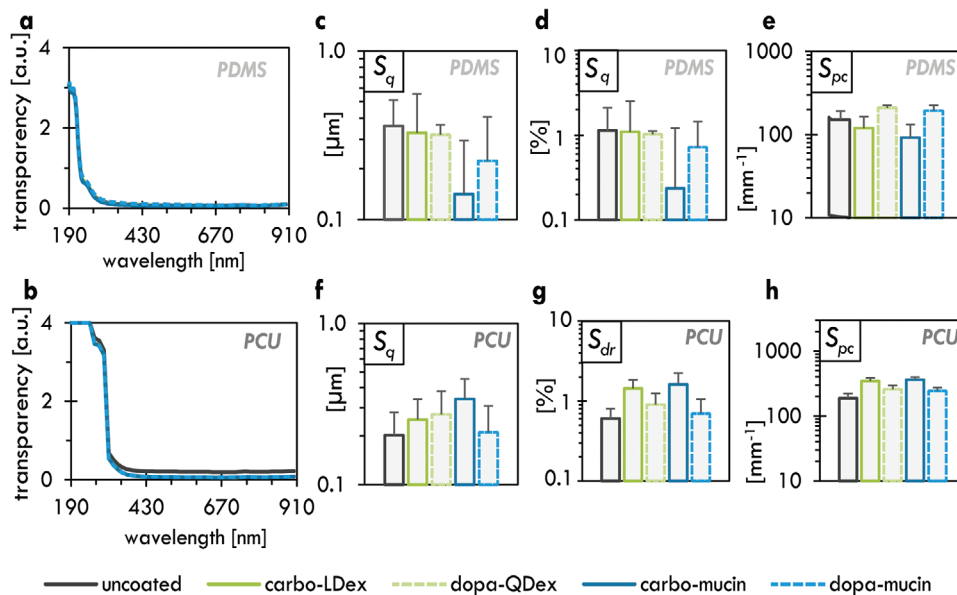


**Figure 4.** Transparency and surface roughness of uncoated and coated PDMS and PCU foils. a,b) Absorbance behavior of the samples in the UV–vis range. c–h) Metrological parameters quantifying different features of the foil surfaces: the root-mean-square-height  $S_q$  (c, f), the developed interfacial ratio  $S_{dr}$  (d, g), and the arithmetic mean peak curvature  $S_{pc}$  (e, h) are compared. All diagrams display results for uncoated samples (black lines), carbo-LDex coated samples (full green lines), dopa-QDex coated samples (dashed green lines), carbo-mucin coated samples (full blue lines), and dopa-mucin coated samples (dashed lines). The legend at the bottom of the figure applies to all diagrams. Error bars depict the error of the mean as determined from at least 6 samples. If no error bars are visible, they are in the range of the size of the symbols.

To compare the flexibility of the foils before and after coating, we determine the torque required to twist a foil sample and compare the surface topography of each sample before and after such a twisting experiment. Again, our aim is to test whether the coating application changes the material behavior rather than interpreting the absolute values obtained from those measurements. Thus, to ensure optimal comparability of the results obtained with different samples, all measured torque values are normalized to the cross-section of the corresponding sample. Similarly, we only evaluate the difference between the determined surface roughness parameters before and after torque application.

Our first observation is that all tested foil samples (i.e., uncoated and coated ones) show a similar overall behavior: at first, the measured torque values are comparably high; then, they decrease within  $\approx 1$  min to a plateau value, which is maintained for the rest of the measurement (which had a total duration of 10 min). To facilitate a quantitative comparison of those time-dependent results, we focus on the initial torque value (Figure 5a, c) as well as the plateau value (Figure 5b, d), which we determine as the mean of all torque values recorded after 60 s. For the initial torque values, we find no significant differences between the coated samples and the uncoated samples, respectively (and this holds true for both, PDMS and PCU samples).

Moreover, for all samples, the drop in the torque values (from the initial value to the plateau value) is about one magnitude of order. Thus, all measured plateau values are very similar—only the results obtained for the PCU-carbo-mucin samples are slightly lower than the values determined for uncoated PCU samples. Accordingly, we find no significant differences when we compare the change in the surface texture of the foil samples: neither when analyzing the height parameter  $S_q$  (Figure 5e, g) nor

when investigating the hybrid parameter  $S_{dr}$  (Figure 5f, h), we find significant differences between any of the coated samples and the respective uncoated control samples. This result is confirmed when we compare the width of the foil samples before and after the flexibility testing (Figure 5 i, k): here, we detect no sign of plastic deformation/narrowing as the results obtained for coated and uncoated samples are virtually identical. Thus, the flexibility of the thin films tested here is not altered by the applied coatings.

Taking into account all the results presented above, we conclude: Eliminating the autohesive behavior of transparent, elastomeric foils is not a trivial task. Here, among the different options tested, the carbo-mucin coating generated on PCU (the material that initially showed the stronger autohesion behavior) achieved this goal best. On PDMS foils, the obtained effects were comparably weak—which is somewhat surprising considering that both substrate materials examined here are transparent, autohesive elastomers with initially similar wettabilities and very similar surface zeta potentials. Our analysis of the surface zeta potentials obtained after different steps of the coating procedures suggests that, for the PDMS samples, the initial surface properties cannot be fully altered even if the coatings are successfully applied. Moreover, we found that, even if eventually the same top-layer macromolecule is applied, the carbodiimide-mediated coatings perform better in reducing the very strong autohesive properties of the PCU samples than dopamine-assisted coatings. For the latter, it seems that the intermediate layer is not fully covered by the macromolecular top layer (even after overnight incubation), which is why (locally) some uncovered, sticky dopamine molecules might still give rise to undesired adhesive properties. Nevertheless, none of the coating variants tested here had any detectable negative impact on the flexibility, transparency, or

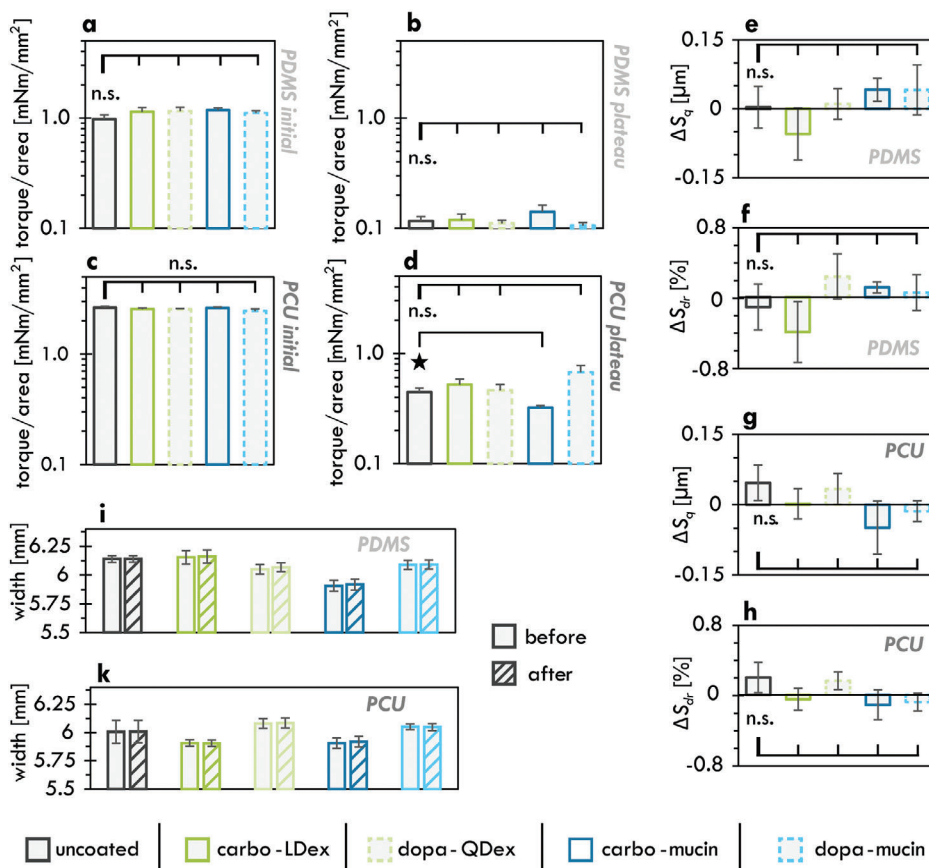


**Figure 5.** Torsional flexibility of bare and coated polymer foils and topographical analysis of the foils after twisting tests. a–d) Torque values determined at the beginning (a, c) and in the plateau phase (b, d) of the flexibility tests. e–h) Differences in the surface roughness parameters  $S_q$  (e, g) and  $S_{dr}$  (f, h) as determined before and after the flexibility tests. i, k) Widths of the foil samples before (empty bars) and after (striped bars) conducting the flexibility tests. All diagrams display results for uncoated samples (black lines), carbo-LDex coated samples (full green lines), dopa-QDex coated samples (dashed green lines), carbo-mucin coated samples (full blue lines), and dopa-mucin coated samples (dashed blue lines). Error bars depict the error of the mean determined from at least 5 samples. Asterisks indicate significant differences ( $p = 0.05$ ); n.s. indicates no significant differences. The legend at the bottom of the figure applies to all diagrams.

roughness of the foils they were generated on—and this is a very promising result.

### 3. Conclusions

Here, we could show that the final surface properties of coated polymeric foils are not only dominated by the properties of the applied top layer-molecules but can still be significantly influenced by the substrate and the selected coating strategy. Two aspects should be kept in mind: first, even though dopamine-based coatings are applicable to a wide range of substrates and can immobilize various top-layer molecules, the intermediate dopamine layer seems to affect the final surface properties of the coated material more strongly than the intermediate layers required for the more complex and more time-consuming carbodiimide-based coatings. Second, the results presented here underscore the importance of choosing a substrate-specific coating strategy on the one hand and a suitable top-layer molecule combination on the other hand—and quantifying the properties of the created coatings in detail is key when tailoring them for a specific application.

### 4. Experimental Section

If not stated differently all chemicals were obtained from Carl Roth, Karlsruhe, Germany.

**Polymeric Materials:** In this study, the following two different polymeric materials were examined:

**Polydimethylsiloxane (Sylard 184, Dow Corning, Midland, MI, USA):** PDMS samples were prepared manually by first mixing PDMS oil in a 10:1 (w/w) ratio with the curing agent and exposing the mixture to vacuum for 1 h to remove air bubbles. The mixture was then filled into a well plate ( $\varnothing$  15 cm, Greiner Bio-One GmbH, Frickenhausen, Germany) such that the PDMS could spread evenly; this process led to samples with a thickness of  $\approx$  300–400  $\mu\text{m}$ . Silicone curing was allowed to take place at 70  $^{\circ}\text{C}$  for 4 h, subsequently, the samples were further tempered at 110  $^{\circ}\text{C}$  for 2 h. Only the surface properties of the side facing the bottom of the well plate during curing were evaluated.

**Polycarbonate-Based Polyurethane (Carbothane AC-4085A, Lubrizol Advanced Materials, USA):** This was a medical grade, polycarbonate-based, thermoplastic, aromatic polyurethane and was extruded by Gerlinger Industries GmbH (Netzschkau, Germany) into foils with a thickness of  $\approx$  150–200  $\mu\text{m}$ ; those foils had a better surface quality on one side, and only the surface properties of this high-quality side were evaluated.

All further preparation steps to shape the samples into the desired dimensions were conducted manually: either they were cut with scissors

and scalpels or punched into a circular shape with a manual eyelet press (Istabreeze Germany GmbH, Bad Rappenau, Germany). Prior to any modifications or tests, all samples were cleaned in 80 % (v/v) ethanol and deionized water (ddH<sub>2</sub>O) for 15 min each and then dried.

**Surface Coatings:** All samples were examined in an uncoated and a coated version. Coatings were applied either via a multi-step carbodiimide-mediated coating process or via a two-step dopamine-based coating process.

**CARBOdiimide-Mediated Coating (carbo):** For this coating process to be feasible on both materials, several coating conditions had to be adjusted to meet the specific properties of each material. Whereas the coating process for PDMS was conducted as published by Winkeljann et al.,<sup>[33]</sup> the process parameters had to be adjusted for the thermoplastic PCU. This was, on the one hand, necessary to achieve a similarly efficient plasma activation on the more resilient PCU; on the other, to compensate for the reduction of the incubation temperature (as PCU has a relatively low Vicat temperature), the concentrations of reactants and/or prolonged treatment times were increased to maintain the efficiency of the multi-step coating procedure. In the following process descriptions, different conditions applied to PDMS and PCU, respectively, will be listed in curved brackets as follows: {applied to PDMS/applied to PCU}.

The surfaces of the samples were activated by applying an atmospheric plasma treatment at a low pressure of 0.4 mbar using a power supply of {30 W/56 W} for {1.5 min/25 min}. As soon as the plasma activation step was completed, each sample was immersed into ≈ 1 mL of a silane solution containing 1 % (w/v) TMS-EDTA (N-[(3-trimethoxysilyl)propyl] ethylenediamine triacetic acid trisodium salt, abcr GmbH, Karlsruhe, Germany) dissolved in 10 mM acetate buffer at pH 4.5 and incubated at {60 °C/37 °C} for {5 h/8.5 h} to create a silane pre-coating. Subsequently, the samples were removed from the silane solution and dipped into isopropanol to wash off any excess solution. To stabilize the silane pre-coating, the samples were exposed to {110 °C & atmospheric pressure/room temperature (RT) & at  $p_{rel} = -800$  to  $-600$  mbar} for {1 h/16 h}. Afterwards, the samples were washed in 96 % (v/v) ethanol on a rolling shaker (≈60 rpm) for 1 h to remove any unbound silane molecules; then, they were dipped into ddH<sub>2</sub>O to wash off any ethanol residues. To initiate the macromolecular coupling step, the samples were immersed into a solution containing 5 mM EDC (1-ethyl-3-(3-dimethylaminopropyl)carbodiimide-hydrochloride) and 5 mM sulfo-NHS (N-hydroxysulfosuccinimid sodium salt, abcr) dissolved in 100 mM MES (2-(N-morpholino)ethanesulfonic acid, AppliChem GmbH, Darmstadt, Germany) buffer at pH 5 (≈ 1 mL per sample). This solution was prepared just before use to avoid preliminary hydrolysis of the coupling agents. Incubation at RT was allowed to take place on a slowly moving tilting shaker for 30 min. Subsequently, the samples were immediately transferred into ≈ 1 mL/sample Dulbecco's phosphate buffered saline (pH = 7.4, DPBS, Sigma-Aldrich Inc., Darmstadt, Germany) containing either 0.05 % (w/v) lysine-dextran (MW = 150 kDa, TdBlabs, Uppsala, Sweden) or 0.05 % (w/v) lab-purified mucins (mainly MUC5AC, which was manually purified from pig stomachs as described by Marczyński et al.).<sup>[34]</sup> During an incubation step of at least 16 h, the samples were slowly moved by a tilting shaker at 7 °C. Once the macromolecular coupling was finalized, to remove unbound macromolecules, the samples were cleaned in 80 % (w/v) ethanol by placing them onto a slowly moving tilting shaker for 30 min.

**DOPAmine-Based Coating (dopa):** For the dopamine coating variant, both materials were treated in the same way. To achieve a smooth and homogenous surface coating, and to prohibit the undesired sedimentation and attachment of larger (poly-)dopamine agglomerates onto the surfaces, the samples were positioned vertically in a suitable coating container, a freshly prepared solution (≈ 1 mL/sample) containing 0.4 % (w/v) dopamine hydrochloride (Sigma-Aldrich) dissolved in 20 mM HEPES buffer (4-(2-hydroxyethyl)-1-piperazineethanesulfonic acid; pH 8.5) was added, and the container was placed onto a slowly moving tilting shaker for 3 h. To wash off excess, not fully attached dopamine, the samples were dipped into ddH<sub>2</sub>O and subsequently immersed into 20 mM HEPES buffer (pH 7) containing either 0.1 (w/v) % Q-dextran (MW = 150 kDa, TdBlabs) or 0.1 % (w/v) of lab-purified mucins. Then, the samples were once more placed onto a slowly moving tilting shaker at RT overnight. To remove any

unbound macromolecules, the samples were dipped into ddH<sub>2</sub>O, into 80 % ethanol, and again into ddH<sub>2</sub>O.

Finally, all samples (independent of how they were coated) were either placed into 20 mM HEPES buffer (pH 7) and stored at 7 °C until further use, or they were dried at RT for at least 24 h (for tests conducted with dry samples).

The specific top-layer molecules studied here were chosen for the following reasons: mucins have recently been introduced as powerful components of coatings for medical devices,<sup>[4,7,35]</sup> and both coating strategies can be used to immobilize those anionic glycoproteins on PDMS and PCU films. As a counterpart for those large biomacromolecules, dextrans were selected, which were also regularly used in biomedical studies—especially as base material for drug delivery applications, and tissue engineering purposes.<sup>[36,37]</sup> Such dextrans were commercially available at different molecular weights and can carry different functionalizations (i.e., charged residues).<sup>[36,38a,38b]</sup> To serve as a positively charged counterpart to the anionic mucin, QDex was chosen due to its strong cationic character (according to the manufacturer) and its strong interaction with dopamine layers which was observed in pretests. However, since such QDex molecules do not possess primary amine groups, applying the carbodiimide-mediated-coating strategy to them was chemically not feasible. Thus, as a suitable alternative, the zwitterionic LDex was used for carbo-coatings since this molecule comprises the same dextran backbone, was available at the same molecular weight, and, at least locally, carries cationic groups.

**Contact Angle Measurements:** CA measurements were conducted using a drop shape analyzer device (DSA25S, Krüss GmbH, Hamburg, Germany). For examining the influence of the coatings on the time-dependent wetting behavior of the materials, dried samples were placed in front of the device-integrated high-resolution camera (ac1920, Basler, Ahrensburg). For imaging, image processing, and image analysis, the device-specific software ADVANCE (AD4021 v 1.13, Krüss GmbH) was used. An automatic imaging protocol was employed that was initiated by a water droplet (6 µL ddH<sub>2</sub>O) crossing a trigger line positioned just above the sample surface. For the first two seconds after triggering, the camera captured images with a frequency of 10 fps. For evaluation, only the first image of the droplet uninfluenced by the cannula as well as the last image of this first series were used. Subsequently, images were captured (each for 1 s at 3 fps) at various additional time steps up to 20 min after the trigger line was crossed. Here, only the second image of each series was evaluated, provided that its quality (sharpness, lighting, no vibration) was sufficient; otherwise, the remaining images served as fallback alternatives. On each image, the CA values were determined as the water-enclosed angle between the surface and the edge of the droplet (using a manually adjusted baseline and the software-integrated Young–Laplace fit method).

**Lap Shear Tests:** For all mechanical examinations, that is, lap shear tests, detachment tests, and flexibility tests, a commercial shear rheometer (MCR 302, Anton Paar, Graz, Austria) equipped with a sample holder unit for disposable bottom plates (P-PTD200/80/I, Anton Paar) was used.

For lap shear tests, two foil samples (≈ 12 mm x 25 mm each) were placed on top of each other such that the overlap region was ≈ 10 mm; then, they manually were pressed together for 10 s, and the contact area was precisely measured using a digital caliper. Both foil samples were inserted into one clamp each and the normal force was reset. Finally, the measuring head was lifted at a velocity of 30 µm s<sup>-1</sup> until both samples fully detached from each other. For comparing the obtained results, the determined force values were divided by the measured contact area to receive a shear stress.

**Detachment Tests:** For adhesion tests, a round foil with a diameter of 10 mm was attached to a commercial PP08 measuring shaft (Anton Paar) using double-sided adhesive tape. First, the zero gap was detected on a disposable aluminum bottom plate (Cat. No. 302 234, Anton Paar), and then a second foil was attached to the bottom plate using double-sided adhesive tape. Afterwards, the normal force was reset, and the shaft was further lowered until a normal force of 5 N was reached, which was maintained for 30 s. Subsequently, reached z-position was held for 60 s to give the foil materials some time to relax. Then, the measuring head was lifted up at a constant speed of 15 µm s<sup>-1</sup>, and a measuring point was recorded every 0.2 s.



**Zeta Potential Measurements:** Zeta potentials were determined for the bare and the coated foil surfaces as well as for the macromolecules (in solution) used as top-layers in the coatings. To ensure comparability of the results, both types of experiments were performed with the same electrolyte solution, that is, ultrapure water containing 1 mM KCl (pH ≈ 5.6).

**Zeta Potential Analysis of Solid Surfaces:** The zeta potentials of solid foil surfaces were determined using a SurPASS 3 Eco device (Anton Paar) equipped with an adjustable gap measuring cell for planar samples (Cat. No. 159 880, Anton Paar). To avoid (re-)hydration effects of the coatings or substrates affecting the measurements in different ways, all samples (i.e., bare, partially coated, or fully coated) were stored in ultrapure water for at least 4 h prior to any measurement. Then the samples were cut into shape (rectangles of 10 mm x 20 mm), and a set of two identical samples was inserted into the measuring cell following the instructions of the device's manufacturer. The gap height was adjusted to a value between 95 and 110 μm and the cell containing the samples was flushed at least twice with the electrolyte solution before a measurement was started at room temperature.

**Zeta Potential Analysis of Macromolecular Solutions:** To assess the zeta potentials of the different macromolecules in solution, the electrophoretic light scattering mode of a LiteSizer500 (Anton Paar) was used. Therefore, an omega cuvette (Mat. No. 155 765, Anton Paar) was filled with the electrolyte solution containing 0.05 % (w/v) of the desired top-layer macromolecule and inserted into the machine. The zeta potentials were then analyzed at 21 °C after an equilibration time of 2 min.

**UV/Vis Measurements:** To examine the influence of the coatings on the transparency of the materials, light absorption measurements in a wavelength range from 190 to 900 nm (in 10 nm steps) were conducted using a microplate reader with cuvette port (SpectraMax ABS Plus, Molecular Devices, LLC, San Jose, US). For each material/coating combination, a UV-cuvette was filled with 1.4 mL of ultrapure water and used as a reference. In those measurements, special care was taken to ensure that all samples were placed at the same position in the laser beam path.

**Confocal Laser Scanning Microscopy:** Confocal laser scanning microscopy was conducted using a VK-X1000 microscope (Keyence, Oberhausen, Germany) equipped with a 20x magnification lens (CF Plan, NA = 0.46; Nikon, Chiyoda, Tokyo, Japan). Prior to performing the measurements, all samples were dried and cleaned with particle-free pressurized air. Then, the samples were placed onto a glass slide using a droplet of distilled water or 80 % (w/v) ethanol as a thin spacer for PCU and PDMS, respectively. This was necessary to allow the measuring device to automatically differentiate between the very thin, transparent foils and the glass slide.

All material/coating combinations were examined before and after subjecting them to torsion tests. At least four samples were analyzed per condition. To determine the full sample width (which later enables a comparison of this sample width before and after the torsion tests), 2x11 images were acquired across the smaller dimension of each sample. To evaluate the surface roughness of the samples (using the software MultiFileAnalyzer (Keyence)), single images were analyzed (by excluding those displaying the edges of the samples). Here, the images were preprocessed as follows: First, a linear tilt based on the full image area was removed; second, the sample waviness (a wave form with correction strength 5 out of 20) was subtracted; third, missing points were filled by estimating the mean height value of the surrounding points. From the adjusted topographical images, the following metrological parameters (based on ISO 25178-2) were calculated: the root-mean-square-height  $S_q$ :

$$S_q = \sqrt{\frac{1}{A} \int \int_A z^2(x, y) dx dy} \quad (1)$$

the developed interfacial ratio  $S_{dr}$ :

$$S_{dr} = \frac{1}{A} \int \int_A \left\{ \sqrt{\left[ 1 + \left( \frac{\partial z(x, y)}{\partial x} \right)^2 + \left( \frac{\partial z(x, y)}{\partial y} \right)^2 \right]} - 1 \right\} dx dy \quad (2)$$

the arithmetic mean peak curvature  $S_{pc}$ :

$$S_{pc} = -\frac{1}{2} \frac{1}{n} \sum_{k=1}^n \left( \frac{\partial^2 z(x, y)}{\partial x^2} + \frac{\partial^2 z(x, y)}{\partial y^2} \right) \quad (3)$$

This set of parameters was chosen as  $S_q$  (which evaluates the height distribution) and  $S_{dr}$  (which describes the relative increase of the determined surface area due to roughness features compared to an entirely planar sample) were frequently used surface roughness parameters that give a good overview over the surface structure of a sample. Additionally,  $S_{pc}$  was selected as a specific parameter evaluating the curvature of the detected peaks; this feature was used to investigate whether any dopamine agglomerates had settled onto the surface as a consequence of the surface modification procedure.

**Torsion Tests:** For torsion measurements, the rheometer was equipped with a measuring shaft for disposable measuring heads (CP/DP70, Anton Paar). To both, the sample holder unit and the measuring shaft, an in-house manufactured aluminum clamp was attached as described in Kimna et al.<sup>[39]</sup> Both clamps were positioned in a parallel orientation, and a foil sample (5 mm x 10 mm) was fixated such that the free length of the samples was always comparable (≈12 mm). The normal force was reset, and the top clamp was moved upwards to pre-stretch the sample until a normal force of -0.3 N was achieved. For the actual torsion measurements, the measuring head performed an oscillating movement over 116.5° to each side at a frequency of 0.2 Hz; measuring points were collected every 0.6 s for a total duration of 10 min. To account for differences in sample thickness, the thickness of each sample was determined using an electronic micrometer screw (Filetta, Schut Geometrische Meettechniek bv, Groningen, Netherlands). The exact width of each sample was determined from the stitched images obtained from confocal laser scanning microscopy (see above). To ensure comparability, all determined torque values were divided by the cross-section (determined by multiplying the sample thickness and width) of the corresponding sample. To examine the influence of the torsional deformation on the material structure, confocal laser scanning microscopy images across the middle section of each sample were captured as described above; images acquired before and after the torsion tests at the same position on each sample were compared.

**Statistical Analysis:** Tests for statistical significance were conducted for all quantitative results shown in Figure 2 and Figure 5. Each set of results was first tested for a normal data distribution using a Shapiro-Wilk test, then, a two-sample F-test was applied to check for equal variances. To test for significant differences between normally distributed samples, a two-sample t-test was applied when the homogeneity of variances was confirmed, whereas a Welch's t-test was performed for heteroskedastic sets of samples. For samples that were not normally distributed, a Wilcoxon-Mann-Whitney test was performed. All statistical analyses were conducted using Microsoft Excel for Microsoft 365 (Version 2206; Microsoft Corporation) employing the add-in Real Statistics Resource Pack software (Release 7.6, Copyright 2013–2021; Charles Zaiantz); differences were considered statistically significant if a *p*-value below 0.05 was obtained.

## Acknowledgements

The authors thank Tobias Fuhrmann for his assistance with the mucin purification and their APRICOT project partners at the Fraunhofer Institute for Manufacturing Engineering and Automation (IPA, Stuttgart, Germany) for procuring and supplying the extruded Carbothane films. This project has received funding from the European Union's Horizon 2020 research and innovation program under grant agreement No 863183. This publication represents the views of the author(s) only. The European Commission is not responsible for any use that may be made of the information it contains.

Open access funding enabled and organized by Projekt DEAL.

## Conflict of Interest

The authors declare no conflict of interest.

## Author Contributions

The study was conceptualized by M.G.B. and O.L.; M.G.B. performed experiments and analyzed the data. The manuscript was written and critically revised by M.G.B. and O.L.

## Data Availability Statement

The data that support the findings of this study are available from the corresponding author upon reasonable request.

## Keywords

carbodiimide coupling, detachment tests, dextrans, dopamine, mucins, surface zeta-potentials

Received: December 6, 2022

Revised: January 25, 2023

Published online: February 20, 2023

- [1] D. C. Rich, *J. Coat Technol. Res.* **2016**, *13*, 1.
- [2] a) M. F. Montemor, *Surf. Coat. Technol.* **2014**, *258*, 17; b) P. A. Sørensen, S. Kiil, K. Dam-Johansen, C. E. Weinell, *J. Coat Technol. Res.* **2009**, *6*, 135.
- [3] A. A. Voevodin, M. S. Donley, J. S. Zabinski, *Surf. Coat. Technol.* **1997**, *92*, 42.
- [4] J. Song, T. M. Lutz, N. Lang, O. Lieleg, *Adv. Healthcare Mater.* **2021**, *10*, 2000831.
- [5] T. Mariappan, *J. Fire Sci.* **2016**, *34*, 120.
- [6] a) M. Cloutier, D. Mantovani, F. Rosei, *Trends Biotechnol.* **2015**, *33*, 637; b) R. O. Darouiche, *Int. Artif. Organs* **2007**, *30*, 820.
- [7] B. Winkeljann, M. G. Bauer, M. Marczyński, T. Rauh, S. A. Sieber, O. Lieleg, *Adv. Mater. Interfaces* **2020**, *7*, 1902069.
- [8] S. Mehla, J. Das, D. Jampaiah, S. Periasamy, A. Nafady, S. K. Bhargava, *Catal. Sci. Technol.* **2019**, *9*, 3582.
- [9] B. Winkeljann, B. T. Käs Dorf, J. Boekhoven, O. Lieleg, *Macromol. Biosci.* **2018**, <https://doi.org/10.1002/mabi.201700311>
- [10] a) C. Kimna, B. Winkeljann, J. Song, O. Lieleg, *Adv. Mater. Interfaces* **2020**, *7*, 2000735; b) F. Siepman, J. Siepman, M. Walther, R. J. Macrae, R. Bodmeier, *J. Controlled Release* **2008**, *125*, 1.
- [11] Y. Liu, G. Wu, K. de Groot, *J. R Soc. Interface* **2010**, *7*, 631.
- [12] a) M. Avella-Oliver, S. Morais, R. Puchades, Á. Maquieira, *Trends Analyt. Chem.* **2016**, *79*, 37; b) M. A. Chowdhury, M. Joshi, B. S. Butola, *J. Eng. Fiber Fabr.* **2014**, *9*, 155892501400900.
- [13] a) M. Samadzadeh, S. H. Boura, M. Peikari, S. M. Kasiriha, A. Ashrafi, *Prog. Org. Coat.* **2010**, *68*, 159; b) F. Zhang, P. Ju, M. Pan, D. Zhang, Y. Huang, G. Li, X. Li, *Corros. Sci.* **2018**, *144*, 74.
- [14] a) L. D. Chambers, K. R. Stokes, F. C. Walsh, R. J. K. Wood, *Surf. Coat. Technol.* **2006**, *201*, 3642; b) F. Guy *Super-Hydrophobic Coatings as a Part of the Aircraft Ice Protection System*, SAE Technical Paper, Warrendale, PA, United States **2017**; c) C. Seubert, K. Nietering, M. Nichols, R. Wykoff, S. Bollin, *Coatings* **2012**, *2*, 221.
- [15] a) E. K. Arya, B. S. Dhanya, *IOP Conf. Ser.: Mater. Sci. Eng.* **2021**, *1114*, 012006; b) B. Shojaei, M. Najafi, A. Yazdanbakhsh, M. Abtahi, C. Zhang, *Polym. Adv. Technol.* **2021**, *32*, 2797; c) C. M. Collins, M. Safiuddin, *Infrastructures* **2022**, *7*, 46.
- [16] a) V. B. Møller, K. Dam-Johansen, S. M. Frankær, S. Kiil, *J. Coat Technol. Res.* **2017**, *14*, 279; b) G. A. Ellis, S. A. Díaz, I. L. Medintz, *Curr. Opin. Biotechnol.* **2021**, *71*, 77; c) S. M. Thomas, R. Dicosimo, V. Nagarajan, *Trends Biotechnol.* **2002**, *20*, 238; d) H. J. Griesser, *Woodhead Publishing Series in Biomaterials*, Woodhead Publishing, Duxford, UK **2016**.
- [17] J. Song, B. Winkeljann, O. Lieleg, *Adv. Mater. Interfaces* **2020**, *7*, 2000850.
- [18] a) P. S. Aklujkar, B. Kandasubramanian, *J. Coat. Technol. Res.* **2021**, *18*, 19; b) M. Kamalisarvestani, R. Saidur, S. Mekhilef, F. S. Javadi, *Renewable Sustainable Energy Rev.* **2013**, *26*, 353.
- [19] a) P. Guan, L. Zhou, Z. Yu, Y. Sun, Y. Liu, F. Wu, Y. Jiang, D. Chu, *J. Energy Chem.* **2020**, *43*, 220; b) A. S. Sarkin, N. Ekren, S. Saglam, *Sol. Energy* **2020**, *199*, 63.
- [20] a) D. J. Miller, D. R. Dreyer, C. W. Bielawski, D. R. Paul, B. D. Freeman, *Angew. Chem., Int. Ed.* **2017**, *56*, 4662; b) A. Rabajczyk, M. Zielecka, W. Kłapsa, A. Dziechciarz, *Materials* **2021**, *14*, 2161.
- [21] K. Czerwinski, T. Rydzkowski, J. Wróblewska-Krepsztul, V. K. Thakur, *Coatings* **2021**, *11*, 1504.
- [22] I. Miranda, A. Souza, P. Sousa, J. Ribeiro, E. M. S. Castanheira, R. Lima, G. Minas, *J. Funct. Biomater.* **2021**, *13*, 2.
- [23] J. Joseph, R. M. Patel, A. Wenham, J. R. Smith, *Trans. IMF* **2018**, *96*, 121.
- [24] F. Awaja, *Polymer* **2016**, *97*, 387.
- [25] P. Boyraz, G. Runge, A. Raatz, *Actuators* **2018**, *7*, 48.
- [26] Y. Choi, H.-V. Tran, T. R. Lee, *Coatings* **2022**, *12*, 1462.
- [27] J. H. Ryu, P. B. Messersmith, H. Lee, *ACS Appl. Mater. Interfaces* **2018**, *10*, 7523.
- [28] a) V. Jokinen, P. Suvanto, S. Franssila, *Biomicrofluidics* **2012**, *6*, 016501; b) M. G. Bauer, R. Reithmeier, T. M. Lutz, O. Lieleg, *Plasma Processes Polym.* **2021**, *18*, 2100126; c) H.-C. Yang, R. Z. Waldman, M.-B. Wu, J. Hou, L. Chen, S. B. Darling, Z.-K. Xu, *Adv. Funct. Mater.* **2018**, *28*, 1705327; d) M. Marczyński, B. Winkeljann, O. Lieleg, in *Biopolymers for Biomedical and Biotechnological Applications*, Wiley, Hoboken **2021**, p. 181; e) R. Bansil, B. S. Turner, *Curr. Opin. Colloid Interface Sci.* **2006**, *11*, 164.
- [29] a) G. Ocvirk, M. Munroe, T. Tang, R. Oleschuk, K. Westra, D. J. Harrison, *Electrophoresis* **2000**, *21*, 107; b) J. K. Beattie, *Lab. Chip* **2006**, *6*, 1409.
- [30] B. J. Kirby, E. F. Hasselbrink, *Electrophoresis* **2004**, *25*, 203.
- [31] R. Zimmermann, U. Freudenberg, R. Schweiß, D. Küttner, C. Werner, *Curr. Opin. Colloid Interface Sci.* **2010**, *15*, 196.
- [32] a) Y. Uematsu, *J. Phys. Condens. Matter.* **2021**, <https://doi.org/10.1088/1361-648X/ac15d5>; b) A. Barisic, J. Lützenkirchen, N. Bebic, Q. Li, K. Hanna, A. Shchukarev, T. Begovic, *Colloids Interfaces* **2021**, *5*, 6; c) Y. Uematsu, D. J. Bonthuis, R. R. Netz, *Curr. Opin. Electrochem.* **2019**, *13*, 166; d) B. J. Kirby, E. F. Hasselbrink, *Electrophoresis* **2004**, *25*, 187.
- [33] B. Winkeljann, P.-M. A. Leipold, O. Lieleg, *Adv. Mater. Interfaces* **2019**, <https://doi.org/10.1002/admi.201900366>
- [34] M. Marczyński, C. A. Rickert, T. Fuhrmann, O. Lieleg, *Sep. Purif. Technol.* **2022**, *294*, 121209.
- [35] a) M. Caldara, R. S. Friedlander, N. L. Kavanaugh, J. Aizenberg, K. R. Foster, K. Ribbeck, *Curr. Biol.* **2012**, *22*, 2325; b) G. Petrou, T. Crouzier, *Biomater. Sci.* **2018**, *6*, 2282; c) C. A. Rickert, B. Wittmann, R. Fromme, O. Lieleg, *ACS Appl. Mater. Interfaces* **2020**, *12*, 28024.
- [36] Q. Hu, Y. Lu, Y. Luo, *Carbohydr. Polym.* **2021**, *264*, 117999.
- [37] S. Tiwari, R. Patil, P. Bahadur, *Polymers* **2018**, *11*, 1.
- [38] a) J. Maia, M. B. Evangelista, H. Gil, L. Ferreira, *Carbohydrates Applications in Medicine*, (Ed: M. H. Gil), Research Signpost, Trivandrum, Kerala, India **2014**; b) W. B. Neely, *Adv. Carbohydr. Chem.* **1960**, *15*, 341.
- [39] C. Kimna, M. G. Bauer, T. M. Lutz, S. Mansi, E. Akyuz, Z. Doganyigit, P. Karakol, P. Mela, O. Lieleg, *Adv. Funct. Mater.* **2022**, *32*, 2105721.